Materials Today Communications 37 (2023) 107270

Contents lists available at ScienceDirect

Materials Today Communications

journal homepage: www.elsevier.com/locate/mtcomm

UV-curable Schiff base-containing polymeric adsorbent for selective and efficient removal of Au(III) from aqueous solutions

Oya Aydın Urucu [a,*], Aslı Beyler Çiğil [b,c,**], Ayşin Zülfikaroğlu [d], Okan Esentürk [c]

[a] Marmara University Faculty of Sciences, Department of Chemistry, Istanbul 34722, Turkey
[b] Gazi University Technical Sciences Vocational, Department of Chemistry and Chemical Process Technology School, Ankara 06374, Turkey
[c] Middle East Technical University Faculty of Arts and Sciences, Department of Chemistry, Ankara 06800, Turkey
[d] Amasya University Faculty of Arts and Sciences, Department of Chemistry, Amasya 05100, Turkey

ARTICLE INFO

Keywords:
Au(III) adsorption
Thiol–ene click reaction
Schiff base
Hydrazone-oxime monomer

ABSTRACT

UV-curable polymeric adsorbent was prepared using a diacrylate-functionalized hydrazone-oxime monomer (DAFHOM), trimethylolpropane triacrylate (TMPTA), and trimethylolpropane tris(3-mercaptopropionate) (TMPTP) through UV-initiated thiol-ene click reaction. Initially, a novel hydrazone-oxime-based Schiff base ligand was synthesized and modified with diacrylate functionality to prepare the UV-curable polymeric adsorbent. The structures of DAFHOM and the resulting polymeric adsorbent were confirmed using Fourier Transform Infrared Spectroscopy (FTIR) analysis. Additionally, the thermal behavior of the UV-cured adsorbent was investigated through thermal gravimetric analysis (TGA), which revealed that the adsorbent exhibited good stability and did not degrade at room temperature. The adsorption performance of the UV-curable polymeric adsorbent for Au(III) from aqueous solutions was studied under various experimental conditions, including pH, contact time, and initial metal concentration. The UV-curable polymeric adsorbent demonstrated effective and selective Au(III) adsorption from aqueous solutions. The findings indicated that removing Au(III) from water solutions positively correlated with pH, particularly within the pH range of 0.5–2.5. However, the efficiency declined when the pH exceeded 1.5. Among the various adsorption isotherm models investigated, the Langmuir model was found to be the most suitable for describing the behavior of the adsorbent. The maximum adsorption capacity of the adsorbent for Au(III) was determined to be 30.06 mg/g. In batch experiments, the UV-curable adsorbent displayed promising selectivity towards Au(III), even in the presence of competitive ions such as Cu (II), Pb(II), and Cd(II).

1. Introduction

Schiff base compounds offer a wide range of reaction conditions from 0° to 100°C. The synthesis of Schiff base products does not require a catalyst, and the resulting products are the desired compounds and water, with no additional by-products. These compounds possess several notable characteristics, including high thermal stability, flame retardancy, and degradability. Consequently, they have found extensive applications in catalyst development, gas separation, and drug release industries [1–3].

Hydrazone-oxime compounds, containing the functional groups –C(O)–NH–N = –CH– and C═N–OH, belong to a class of Schiff Bases [4,5]. These compounds find various applications in the pharmaceutical, analytical, and chemical fields [6]. Hydrazone-oxime Schiff Bases possess multiple potential bonding sites, including carbonyl, imine, and azomethine groups, making them potential chelating ligands [7,8]. Oxygen and nitrogen donor atoms arranged in suitable positions enable these compounds to readily coordinate with metal ions of varying oxidation states [9,10]. Extensive research has been conducted on the coordination complexes of various ligands [7,8]. These ligands belong to two distinct classes of chromogenic chemicals frequently utilized in determining metal ions using derivative spectrophotometry [11]. They serve as significant organic analytical reagents and have been employed to quantify metal ions in actual and simulated samples using

* Corresponding author.
** Corresponding author at: Gazi University Technical Sciences Vocational, Department of Chemistry and Chemical Process Technology School, Ankara 06374, Turkey.
E-mail addresses: oaydinurucu@marmara.edu.tr (O. Aydın Urucu), asli.beyler@gazi.edu.tr (A. Beyler Çiğil).

https://doi.org/10.1016/j.mtcomm.2023.107270
Received 25 September 2023; Accepted 5 October 2023
Available online 6 October 2023

spectrophotometry [12].

Several analytical techniques are available for quantifying metal ions at micro levels, including Fluorescence spectroscopy, inductively coupled plasma atomic emission spectroscopy (ICP-AES), and atomic absorption spectrophotometry (AAS). Flame Atomic Absorption Spectroscopy (AAS) is a widely employed analytical technique for quantifying trace metal concentrations in various materials due to its cost-effectiveness and straightforward and user-friendly nature [13–15]. This approach enables the development of both sequential and simultaneous methods to accurately determine numerous elements with exceptional sensitivity and effective background correction. It enables high-throughput, quantitative analysis of metal content in solid and liquid samples, making it suitable for various applications [16–18]. This method is known to be rapid, sensitive, selective, reproducible, and free from interference by many common metal ions [19].

Gold is a valuable metal with a wide range of applications. From the perspective of global resource sustainability, the recycling of gold from wastewater holds significant importance. Wastewater from mining, jewelry manufacturing, and electronic waste recycling contains trace amounts of gold. Recovering gold from these wastewater streams helps minimize the loss or disposal of this valuable metal [20–22].

However, the separation and recovery of Au(III) from wastewater is not straightforward due to low concentrations, extreme acidity, and complex matrices. Various methods, such as solvent extraction, electrochemical separation, membrane filtration, and adsorption, have been developed to extract Au(III) from aqueous matrices. Among these methods, adsorption is the most suitable and effective technology due to its simplicity, high efficiency, low-cost setup, and minimal secondary waste [18,22].

Different polymeric adsorbent studies are prepared for determining Au(III) in the literature [23–25]. However, such studies have disadvantages, such as toxic solvents, complex procedures, undesirable by-product formation, expensive materials, and time-consuming procedures. Therefore, in this study, we preferred to use click reactions, which have become prominent in materials science in recent years, to prepare the adsorbent. Click reactions offer numerous advantages compared to other methods. They have a broad scope, high efficiency, and generate only harmless by-products that can be easily removed without chromatography. Click reactions are also stereospecific, simple to perform, and do not require high energy or solvents that are difficult to remove [26,27]. Several reactions fulfill the criteria for click chemistry, including thiol-ene and Diels-Alder chemistry, as well as carbonyl-condensations involving oxime, imine, and hydrazone functionalities. These click reactions exhibit desirable properties such as high efficiency, specificity, ease of synthesis, and straightforward purification, making them attractive alternatives to conventional methods' complex, costly, and time-consuming procedures [28,29]. Materials with superior performance can be achieved by employing highly efficient click chemistry instead of traditional chemical reactions.

Recently, the applications of carbonyl click chemistry, specifically imine, hydrazone, and oxime reactions, have gained popularity in polymer/materials science due to their exceptional efficiency, bio-orthogonal nature, and dynamic covalent properties. Both imine and hydrazone reactions have been utilized for polymer synthesis and functionalization and developing self-healing and degradable materials [30–32]. However, the potential of the oxime click reaction in polymer science remains largely unexplored. The favorable characteristics of oxime bond formation, including high efficiency, chemo selectivity, compatibility with aqueous solvents, and water as the sole by-product, provide significant advantages for its utilization in various applications. The thiol-ene click reaction was used for the first time in the literature to form a metal adsorbent by integrating the hydrazone-oxime ligand into a cross-linked network structure.

The present study aimed to prepare a UV-curable polymeric adsorbent that can selectively and efficiently adsorb Au(III) ions in aqueous solutions. The UV-curable polymeric adsorbent was prepared from Schiff base-containing diacrylate-functionalized hydrazone-oxime monomer, trimethylolpropane triacrylate, and trimethylolpropane tris (3-mercaptopropionate) by UV initiated thiol-ene click reaction. The adsorbent was prepared for the first time in the literature by using thiol-acrylate and hydrazone-oxime click reactions together. This way, flexible, cross-linked adsorbents were obtained quickly without toxic solvents. Additionally, the nitrogen atoms of oxime and azomethine groups on the surface of the obtained UV-curable adsorbent can selectively combine with Au(III) ions. When compared to the adsorptions of Cd(II), Pb(II), or Cu(II), the adsorbent exhibited approximately 60 times greater selectivity.

2. Experimental section

2.1. Materials and apparatus

Acetophenone (Fluka), isopentyl nitrite (Fluka), metallic sodium (Fluka), 4-Hydroxybenzoylhydrazine (Merck), glacial acetic acid (Sigma-Aldrich), absolute ethanol (Sigma-Aldrich) was used in the synthesis of isonitrosoacetophenone 4-hydroxybenzoylhydrazone ($inafhbH_2$) without further purification. 2-Isocyanatoethyl methacrylate (IEM) (Sigma-Aldrich) was used in the modification of isonitrosoacetophenone hydroxybenzoylhydrazone ($inafhbH_2$). Trimethylolpropane triacrylate (TMPTA) (Sigma-Aldrich), trimethylolpropane tris(3-mercaptopropionate) (TMPTP) (Sigma-Aldrich), 2-hydroxy-2-methyl-1-phenyl-propan-1-one (Irg 2022, photoinitiator) (Sigma-Aldrich) were used in the synthesis of UV-curable polymeric adsorbent.

2.2. Synthesis of the $inafhbH_2$

Isonitrosoacetophenone was synthesized following the procedure described in the literature [33]. Isonitrosoacetophenone (2 mmol, 0.304 g) and 4-hydroxy benzoyl hydrazine (2 mmol, 0.298 g) were dissolved in 30 mL of absolute ethanol and then refluxed for 10 h with the addition of eight drops of glacial acetic acid. Subsequently, 60 mL of distilled water was introduced to the reaction mixture, and the mixture was refrigerated overnight. The resulting white precipitate was filtered and washed successively with water, ethanol, and diethyl ether. Scheme 1 illustrates the synthesis of $inafhbH_2$. Yield: 75%, Melting point: 201 ℃, Elemental analysis of CHN ($C15H13N3O3$: 283.29 g mol^{-1}): Found (Calcd.)(%): C:62.99 (63.60), H:5.01 (4.63), N:15.01 (14.83).

2.3. Synthesis of the diacrylate-functionalized hydrazone-oxime monomer (DAFHOM)

The diacrylate-functionalized hydrazone-oxime monomer (DAFHOM) was synthesized following the method proposed by Sang et al. [34]. The reaction was conducted under a nitrogen (N_2) atmosphere. Initially, 2.5 g (8.8 mmol) of $inafhbH_2$ hydrazone-oxime compound was dissolved in 80.0 mL of toluene with magnetic stirring. Subsequently, 2.73 g (17.6 mmol) of IEM was added to the reaction mixture, stirring at 80 °C for 5 h. Upon completion, toluene was evaporated from the reaction system, yielding a yellow solid. The resulting product was washed three times with distilled water to remove excess $inafhbH_2$ hydrazone-oxime compound. Finally, the precipitate was dried under a vacuum at 40 °C for 18 h.

The scheme of the synthesis of the diacrylate-functionalized hydrazone-oxime monomer (DAFHOM) is shown in Scheme 1.

2.4. Preparation of UV–curable polymeric adsorbent

A mixture of TMPTA (1 g), TMPTP (4 g), and DAFHOM (1 g) was placed in a beaker covered with aluminum foil. The mixture underwent ultrasonic treatment in a bath for 15 min to ensure homogeneity. Subsequently, the photoinitiator (0.18 g, 3% by weight) was added to the

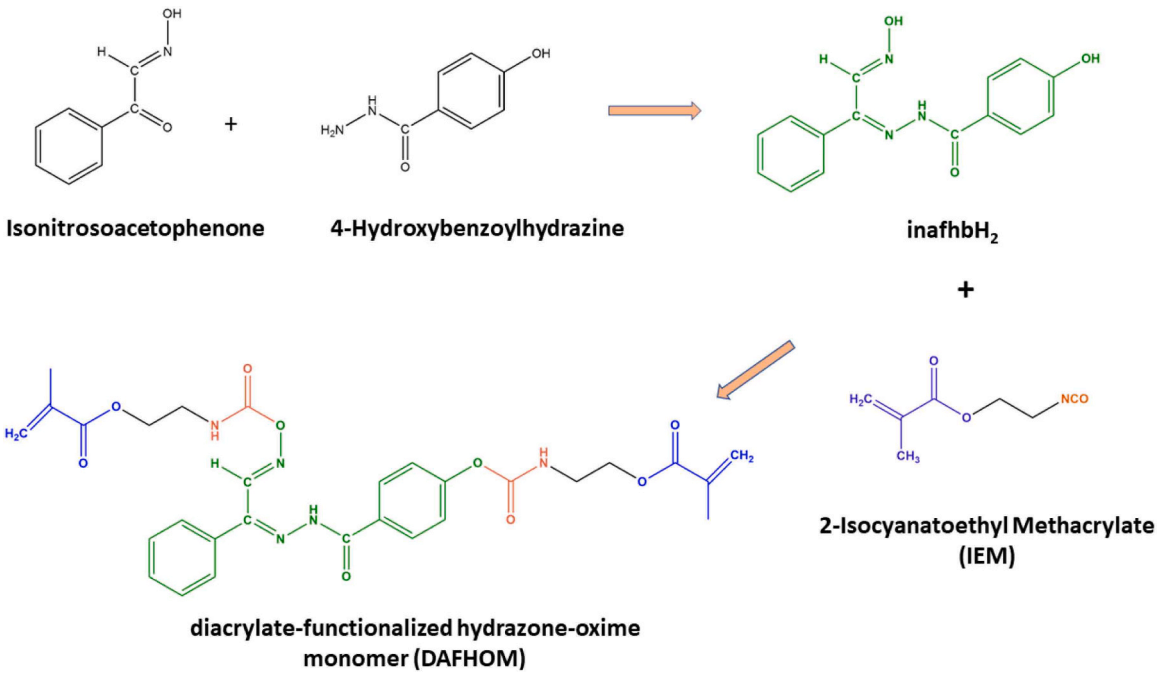

Scheme 1. The synthesis schematic of the diacrylate-functionalized hydrazone-oxime monomer.

mixture. Finally, the combined solution was poured into a polytetrafluoroethylene mold and exposed to UV light for 3 min, facilitating the thiol-acrylate click reaction. Scheme 2 visually illustrates the procedure for preparing the UV-curable adsorbents.

2.5. Characterization

Fourier Transform Infrared Spectroscopy (FTIR) spectra were obtained for inafhbH$_2$ using the KBr pellet technique on a PerkinElmer FTIR spectrometer in the 4000–400 cm^{-1} range. Additionally, FTIR spectra of TMPTA, TMPTP, DAFHOM, and UV-curable adsorbent were recorded on a Thermo Nicolet iS10 spectrometer in the range of 4000–600 cm^{-1} to confirm their structures.

The ^{1}H and ^{13}C NMR spectra of inafhbH$_2$ were acquired using a Bruker DPX-400 FT NMR spectrometer in DMSO-d^{6}.

Thermal gravimetric analysis (TGA) of the UV-curable adsorbent was performed using a Perkin Elmer Instrument, STA6000. The sample was heated from 30° to 750°C at 10 °C/min under an air atmosphere.

The morphology of the UV-curable adsorbent was examined with a Carl-Zeiss Evo40 Scanning Electron Microscope (SEM). Before analysis, the UV-curable adsorbent was fractured and coated with a 20 nm layer of gold/palladium using sputter coating to enhance conductivity and prevent charging during the project. SEM was conducted at a constant electron high tension voltage of 15 kV in a high vacuum chamber. Moreover, the elemental composition of the UV-curable adsorbent surface was determined using energy-dispersive X-ray spectroscopy (EDAX).

The UV-curable adsorbent's water contact angles (WCAs) were measured at room temperature using an Attension Theta Lite optical tensiometer. Distilled water droplets of 3–5 μL were employed for the measurements, and five measurements were taken to calculate the average value of the contact angles. Image analysis was performed to determine the right accurately and left WCAs with a precision of ± 0.14°.

A flame atomic absorption spectrophotometer, specifically the Analytik Jena Zeenit 700 model from Jena, Germany, was utilized to experiment. Continuous background correction was ensured by fitting the instrument with a deuterium lamp.

2.6. Adsorption of the Au(III) ions

Batch mode adsorption studies of Au(III) ions were conducted at

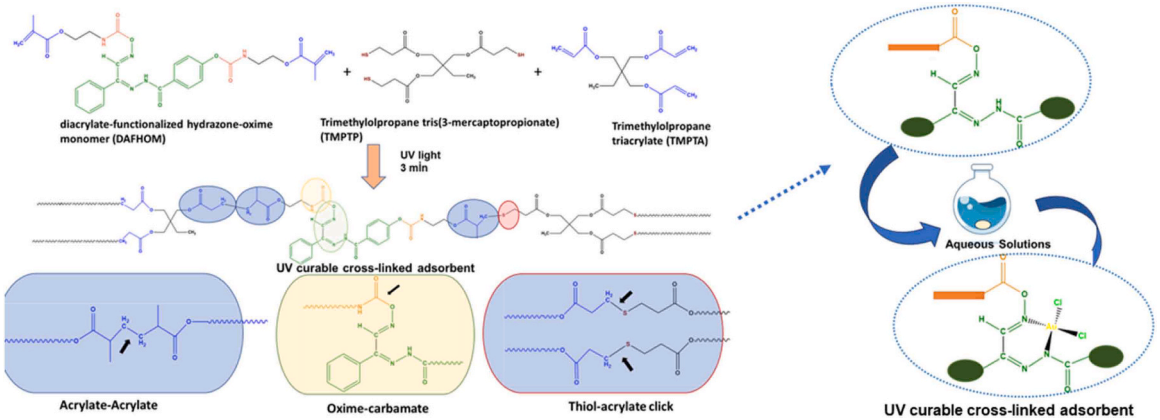

Scheme 2. Preparation of UV-curable adsorbents and illustration of the interaction of the Au(III) ions with the UV-curable adsorbent.

room temperature with constant shaking at 150 rpm. The initial pH of the Au(III) solutions and the contact time parameters were considered influential factors in the adsorption process. The removal of Au(III) ions was quantified using Flame Atomic Absorption Spectrometry. All adsorption experiments utilized 20 mL of 30 mg/L metal solutions and approximately 35 mg of the adsorbent. The pH study encompassed a 6-hour duration in the pH range of 0.5–2.5. Dilute HCl and NaOH solutions were employed for pH adjustments. The investigation of the optimal contact time spanned between 1 and 8 h. For isotherm studies, the pH was set to 1.5, and a range of 10–210 mg/L of Au(III) ions was used for 6 h.

Using the provided equation, the adsorption capacities of the synthesized UV-curable adsorbent for Au(III) ions were subsequently calculated [18].

$$q_e = \left(\frac{C_0 - C_e}{m.1000}\right).V \quad (1)$$

In the adsorption process, the variables are defined as follows: C_0 represents the initial concentration of Au(III) ions (mg/L), C_e denotes the remaining Au(III) ion concentration after the process (mg/L), V stands for the volume of the Au(III) ion solution (mL), q_e represents the adsorption capacity of the UV-curable adsorbent (mg/g), and m represents the amount of UV-curable adsorbent used (g).

3. Results and discussion

3.1. Structural characterization of the diacrylate-functionalized hydrazone-oxime monomer (DAFHOM)

In the ^{1}H NMR spectra of inafhbH$_2$ (Fig. S1a), characteristic resonances due to OH and NH protons, associated with oxime and hydrazone groups, appeared at 12.65 ppm and 13.28 ppm as singlets, respectively. The signals assigned to the phenolic OH and CH (–CH=NOH) protons were observed at 10.35 ppm and 8.52 ppm, respectively. Additionally, signals in the 7.80–6.91 ppm range were assigned to the aromatic protons of phenyl rings. Upon reaction with IEM, the ^{1}H NMR of the diacrylate-functionalized hydrazone-oxime monomer exhibited new peaks in both the downfield and upfield regions. Notably, the reaction with 2-isocyanate ethyl methacrylate resulted in the complete disappearance of the phenolic OH peak, and the previously absent 1.84 peaks were attributed to the methylene group of IEM. Furthermore, the protons of acrylate double bonds resonated around 6.5–6.1 ppm (Fig. S1c).

In the ^{13}C NMR spectra of inafhbH$_2$ (Fig. S1b), signals at 161.73 ppm, 145.79 ppm, and 136.82 ppm were assigned to (C═O), (C═N)$_{oxime}$, and (C═N)$_{azomethine}$, respectively, confirming the structure of inafhbH$_2$. Signals in the 140.67–115.57 ppm region corresponding to carbon atoms in phenyl rings were also observed. The ^{1}H and ^{13}C NMR results of inafhbH$_2$ were consistent with data from similar compounds [35–38].

The confirmation of a successful reaction was conducted using FTIR analysis. Fig. 1 presents the FTIR spectrum of the inafhbH$_2$ compound. The spectrum exhibited a broad band ranging from 3400 to 3100 cm^{-1}, indicating NH stretching vibration and the oxime group's OH stretching vibration [35,39]. Furthermore, the OH stretching vibration of phenol was observed at 3544 cm^{-1}. Peaks at 1639 cm^{-1}, 1606 cm^{-1}, and 1536 cm^{-1}were assigned to the characteristic stretching vibrations of the amide carbonyl (C═O), (C═N)$_{azomethine}$, and (C═N)$_{oxime}$ groups, respectively [5,9,10].

Comparatively, the FTIR spectra of the diacrylate-functionalized hydrazone-oxime monomer closely resembled that of the inafhbH$_2$ compound, except for some new peaks. Notably, peaks at 2960 and 2880 cm^{-1} indicated the stretching of CH_3 and CH_2 from IEM, while the peak at 1631 cm^{-1} was attributed to the double bond of the methacrylate group from IEM. Furthermore, the peak at 1700 cm^{-1}corresponded to the carbonyl group stretching from IEM. These findings strongly suggest a reaction between inafhbH$_2$ and IEM, resulting in the successful incorporation of methacrylate groups into inafhbH$_2$.

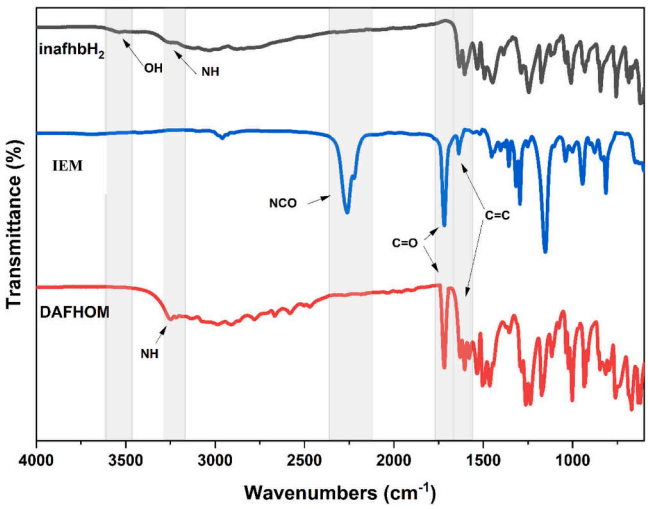

Fig. 1. FTIR spectrum of the inafhbH$_2$, IEM and DAFHOM.

3.2. Structural characterization of the UV-curable adsorbent

The UV-curable adsorbent was structurally characterized using FTIR spectroscopy. Fig. 2 shows the FTIR spectrum of the synthesized UV-curable adsorbent, as well as the spectra of trimethylolpropane tris(3-mercaptopropionate) (TMPTP), trimethylolpropane triacrylate (TMPTA), and diacrylate-functionalized hydrazone-oxime monomer.

The FTIR spectra exhibit characteristic bands at approximately 2960 cm^{-1} and 2920 cm^{-1}, arising from stretching aliphatic -CH- bonds. Furthermore, peaks around 1700 cm^{-1} are observed, corresponding to the stretching vibrations of carbonyl groups present in TMPTP, and TMPTA. Additionally, the FTIR spectrum of the UV-curable adsorbent shows characteristic bands associated with N-H and C═O bonds originating from the amide functionality present in DAFHOM. It exhibits moderate to strong bands at 3302 cm-1 and 3112 cm-1, characteristic of the N-H functional group. In addition, in the FTIR spectrum of the UV-curable adsorbent, bands belonging to (C═N)$_{azomethine}$, and (C═N)$_{oxime}$ groups are seen at 1606 cm-1, and 1557 cm-1, respectively, originating from the DAFHOM monomer. Since the nitrogen atoms of the oxime and azomethine groups on the surface of the adsorbent can selectively combine with Au(III) ions, it is important that these functional groups are seen in the FTIR spectrum [40–42]. Illustration of the interaction of the Au(III) ions with the UV-curable adsorbent (Scheme 2). Upon UV irradiation, thiol-acrylate reactions occur, wherein thiol groups react with the acrylate functional groups via a photoinduced step-growth mechanism. Consequently, both the thiol and acrylate bands disappear, indicating the successful completion of the photocuring process. These findings are consistent with the information reported in the literature [43,44].

3.3. Thermal stability of the UV-curable adsorbent

Thermal properties of the UV-curable adsorbent were characterized by TGA analysis. Fig. 3 shows the TGA thermogram of the adsorbent film in air.

The results indicated that the UV-curable adsorbent in an air atmosphere is thermally stable below 300 °C but rapidly decomposes at temperatures between 300 and 600 °C (T_{max1} = 333 °C, T_{max2} = 455 °C, and T_{max3} = 572 °C). The initial reduction in weight can be attributed to the elimination of residual uncured low molecular-weight components (extractable substances). Between 450 and 520 °C, a sharp weight decline of 91.6% was observed for the adsorbent, which was associated

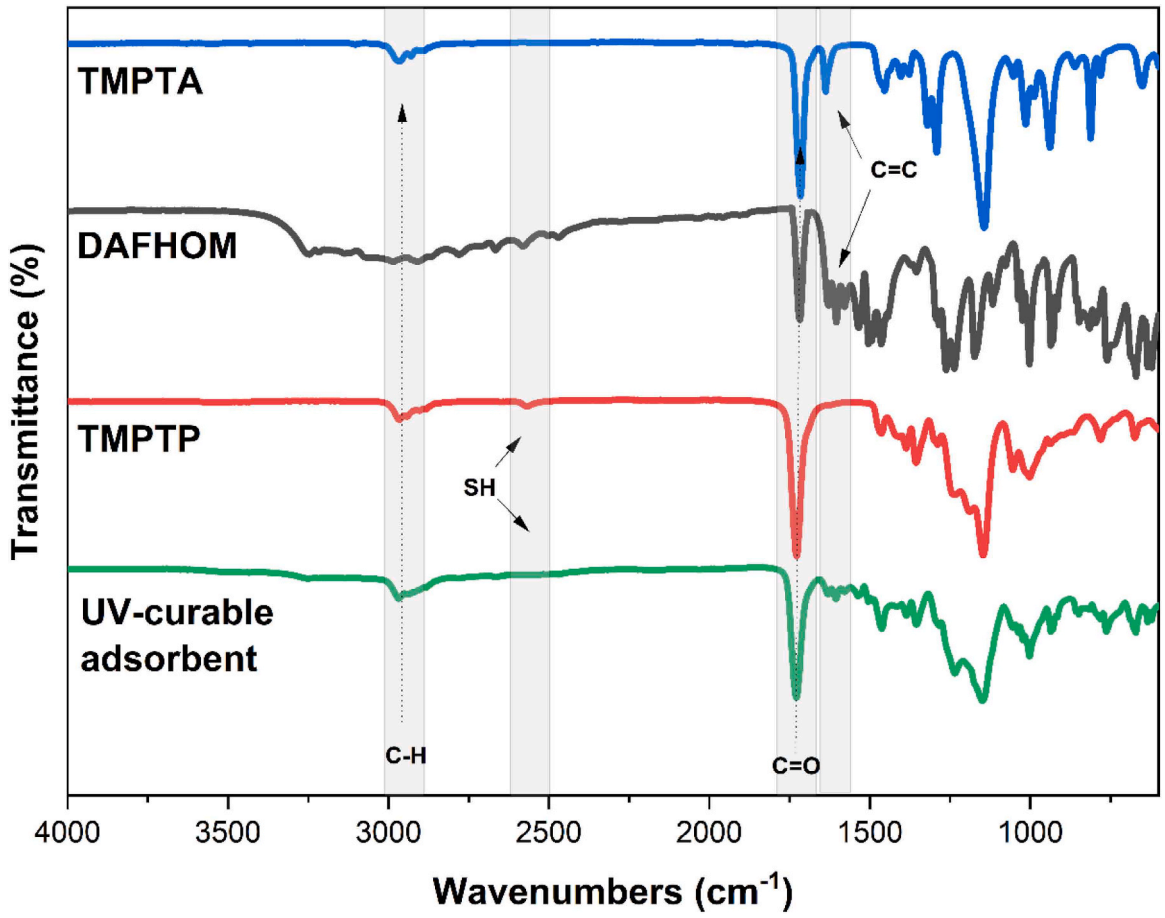

Fig. 2. FTIR spectrum of TMPTP, TMPTA, DAFHOM, and UV-curable adsorbent.

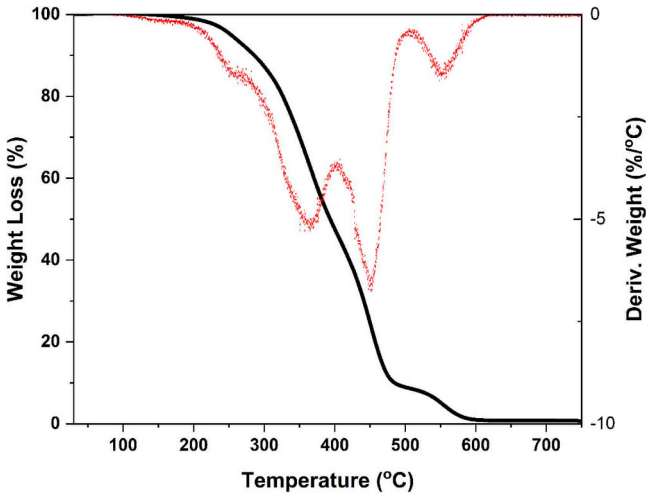

Fig. 3. TGA thermogram and the derivative weight curve of the UV-curable adsorbent.

with the cleavage of strong covalent bonds and the destruction of the polymeric chain. The UV-curable adsorbent exhibits a significant weight loss after 300 °C, demonstrating its relative stability and resistance to degradation at normal temperatures.

3.4. Morphological properties of the UV-curable adsorbent

The morphological characteristics of the UV-curable adsorbent were investigated and compared using SEM images of the samples. Fig. 4a-d display SEM images of the fractured surfaces of the adsorbent at varying magnification levels. These images confirmed a homogeneous distribution of diacrylate-functionalized hydrazone-oxime, TMPTA, TMPTP, and the photoinitiator within the matrix. The SEM images suggest a highly cross-linked, non-porous network structure in all the films.

To determine the chemical composition of the UV-curable adsorbent, SEM-EDAX analysis was conducted. Fig. 4e illustrates the presence of distinct peaks of sulfur (attributed to TMPTP) and nitrogen (associated with diacrylate-functionalized hydrazone-oxime). Carbon and oxygen peaks were also detected, along with gold and platinum peaks associated with the gold-platinum coating applied to the adsorbent. The carbon and oxygen peaks were considered to originate from both the sample and adsorbents from the air.

The previous studies on metal absorbents prepared via the thiol-ene click reaction under UV irradiation were examined and it was seen that their SEM images exhibited similarities to those obtained in the present study. Fırlak et al. (2014) explored the adsorption of Au(III) ions from geothermal waters using a hydrogel prepared by the thiol-ene click reaction under UV irradiation [45]. The hydrogels were synthesized from pentaerythritol tetrakis (3- mercaptopropionate), acrylic acid, and poly (ethylene glycol) dimethacrylate. Similar to our findings, the SEM images of the hydrogels showed a non-porous network. In a separate study, an environmentally friendly adsorbent was synthesized using cellulose acetate butyrate and cysteine through a thiol-ene click reaction under UV irradiation to efficiently recover Ag(I) ions from actual streams and lake waters [46]. Upon examining the SEM images of this eco-friendly adsorbent, a resemblance was observed with the SEM images obtained in our present study.

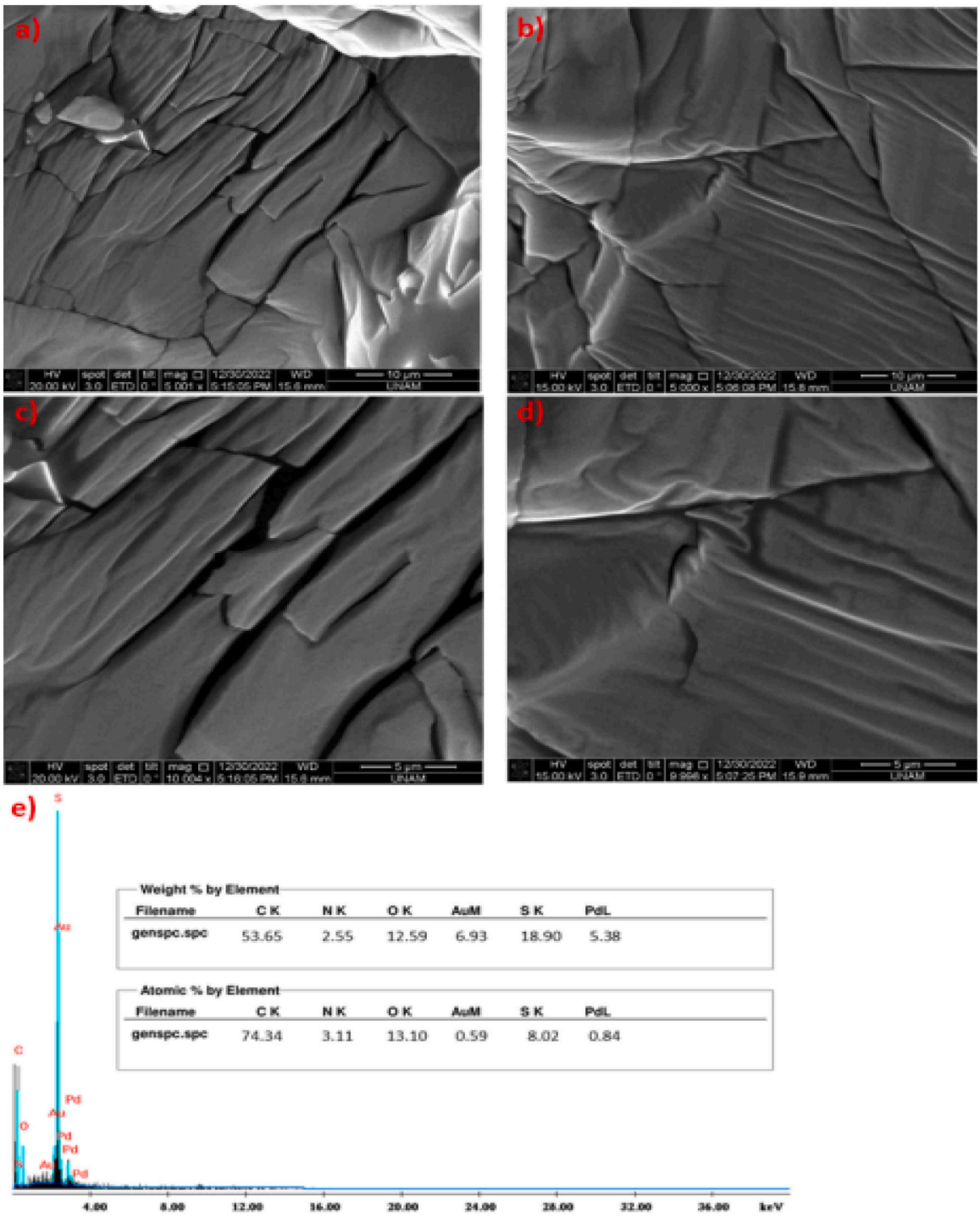

Fig. 4. UV-curable adsorbent a) SEM image x 5000, b) SEM image x 5000, c) SEM image x 10000 d) SEM image x 10000, and e) EDAX analysis and elemental composition.

3.5. *Wettability of UV-curable adsorbent*

The hydrophilic/hydrophobic character of the UV-curable adsorbent was examined by measuring the water contact angle (WCA) values. The average WCA value of UV-curable adsorbent was $101.4 \pm 0.14^{\circ}$. The image is given in Fig. S4. The observed expected value can be attributed to the absence of unreacted hydrophilic groups within the cross-linked polymeric network. The augmentation of hydrophobicity, as evident from the increase in water contact angle, signifies the prepared adsorbent's remarkable stability in aqueous environments, rendering it suitable for conducting adsorption studies [47].

3.6. *The effect of pH*

The pH of the aqueous medium is a crucial parameter in adsorption processes and can affect the electrostatic charge balance on the adsorbent's surface. The effect of pH on the adsorption of Au(III) ions on a UV-curable adsorbent was investigated by varying the pH from 0.5–2.5.

Au(III) ions are predominantly present in aqueous solutions as $Au(H_2O)_4^{3+}$. In the case of stronger ligands such as Cl^{-}, the equilibrium [18,

48] is established as follows:

$$Au(H_2O)_4^{3+}\ (aq) + 4\ Cl^-\ (aq) \leftrightarrow AuCl_4^-\ (aq) + 4\ H_2O \quad (2)$$

The present study examined the effect of pH on the adsorption of [$AuCl_4^-$] ions onto the UV-curable adsorbent within a pH range of 0.5–2.5. Accordingly, a 35 mg UV-curable adsorbent was utilized. The results indicated that the UV-curable adsorbent demonstrated greater effectiveness in adsorbing [$AuCl_4^-$] ions under strongly acidic conditions than in slightly acidic environments. The highest adsorption of [$AuCl_4^-$] onto the UV-curable adsorbent was observed at pH 1.5, as presented in Fig. 5.

3.7. Effect of contact time

The contact time during the metal adsorption process onto the polymer surface is essential for the adsorption kinetics. The adsorption of metal ions onto the polymer surface occurs during the contact time, and sufficient time is required to reach the maximum adsorption capacity [45,49]. A short contact time does not allow enough adsorption of metal ions onto the polymer surface and results in a low adsorption capacity. On the other hand, an excessively long contact time is unnecessary and leads to time and energy waste after the adsorption reaches saturation. Therefore, determining an appropriate contact time can achieve the maximum adsorption capacity for the metal ions to be adsorbed onto the polymer surface. In this study, the contact time was 6 h for the adsorption of Au(III) ions onto the UV-curable adsorbent (Fig. 6).

3.8. Effect of initial metal concentration

To determine the adsorption capacity of Au(III) ions on the adsorbent, an investigation was conducted using approximately 35 mg of adsorbent at pH 1.5, with varying initial Au(III) concentrations ranging from 1 to 210 mg/L over 6 h. Fig. 7 shows that adsorption capacity increases with the rising initial concentration of Au(III) ions. The maximum adsorption capacity of 30.06 mg/g was achieved at a low 80 mg/L concentration.

3.9. Adsorption isotherms

Adsorption isotherms can be employed to characterize the adsorption behavior of a material and determine the parameters governing the adsorption process. Isotherms such as Langmuir, Freundlich, Temkin, Dubinin, and Radushkevich can provide valuable insights into the type of adsorption mechanism at play [18,45,48,50].

The Langmuir adsorption isotherm assumes that adsorption occurs at specific sites on the surface of the adsorbent and that the maximum amount of adsorption possible is limited by the number of available sites.

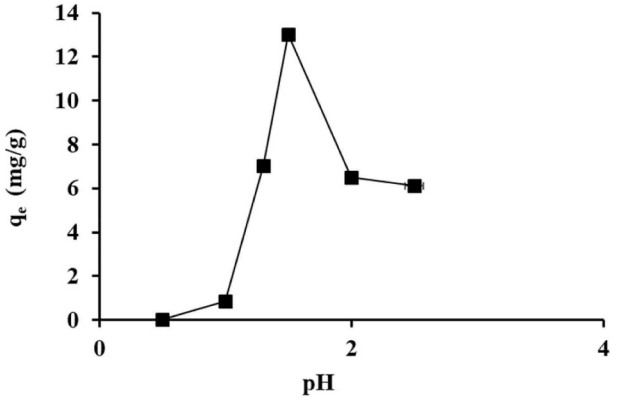

Fig. 5. The effect of pH (35 mg adsorbent N:3).

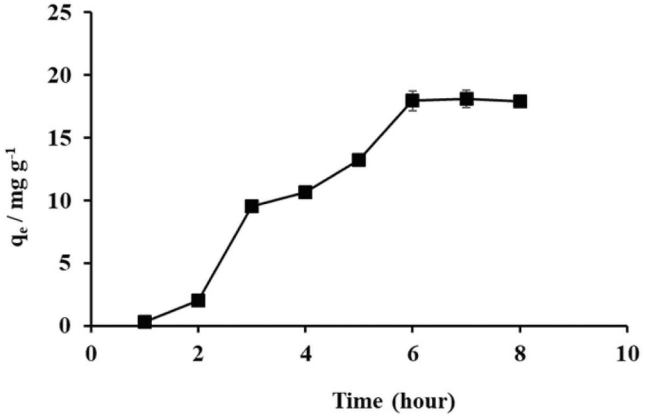

Fig. 6. The effect of contact time (35 mg adsorbent, pH:1.5 N:3).

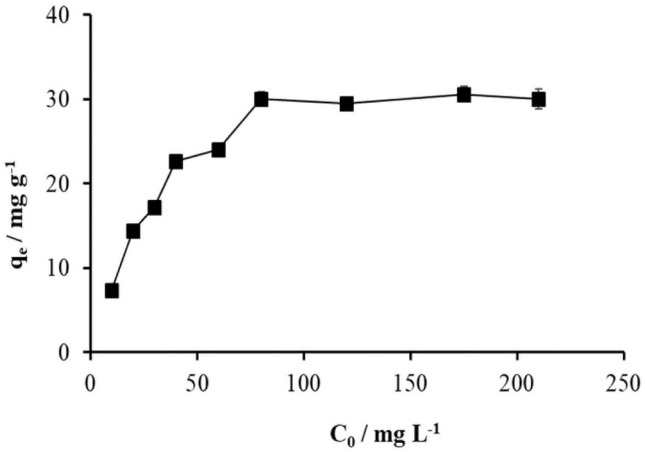

Fig. 7. The effect of initial Au(III) concentration (35 mg adsorbent, pH:1.5 N:3).

$$\frac{C_e}{q_e} = \frac{C_e}{q_{max}} + \frac{1}{q_{max} K_L} \quad (3)$$

The separation factor constant (R_L) values, which provide an indication of the feasibility of the adsorption process, were employed to assess the suitability of hydrogels for gold ion adsorption. R_L values greater than 1.0 suggest unsuitability, R_L equal to 1 indicates linearity, R_L values between 0 and 1 suggest suitability, and R_L equal to 0 implies irreversibility. The R_L value can be calculated using the following equation:

$$R_L = \frac{1}{1 + C_o K_L} \quad (4)$$

q_{max}: Maximum adsorption capacity (mg/g) K_L: Langmuir constant C_0: (mmol/ L) is the initial concentration of Au (III) ions.

The Freundlich isotherm can be applied over a wide range of concentrations and be used in cases where the adsorbent has a heterogeneous structure.

$$\ln q_e = \frac{1}{n} \ln C_e + \ln K_f \quad (5)$$

1/n and K_f: Empirical constants.

According to the Temkin isotherm, the decrease in adsorption heat of all molecules occurs linearly, indicating homogeneous binding energy.

$$q_e = B_T \ln K_T + B_T \ln C_e \quad (6)$$

B_T: Temkin constant K_T (L/g): Equilibrium binding constant.

Dubinin and Radushkevich (D-R) isotherm is based on the potential theory of a heterogeneous surface

$$lnq_e = lnq_{\max} - K_{DR}\varepsilon^2 \quad (7)$$

K_{DR}: Dubinin-Radushkevich isotherm constant, ε: Polanyi potential.

The average adsorption energy (E) helps us to predict the adsorption mechanism.

$$E = \frac{1}{\sqrt{2K_{DR}}} \quad (8)$$

The average adsorption energy (E) aids in predicting the adsorption mechanism. If the E value falls within the range of 8–16 kJ/mol, the adsorption process is characterized by ion exchange. For E values less than 8 kJ/mol, physical adsorption is predominant, while for values between 20 and 40 kJ/mol, chemical adsorption can be considered.

Table 1 summarizes the data obtained from the isotherm studies (Fig. S2a-d). The Langmuir isotherm showed a substantially higher correlation coefficient than the other isotherms, indicating that this isotherm best describes our adsorption process. This implies the occurrence of a single-layer chemical adsorption process, signifying the existence of uniform adsorption sites on the adsorbent. Additionally, the separation factor constant (R_L), which is important for the Langmuir isotherm, was found to be 0.801. Since these values fall within the range of $0 < RL < 1$, it has been determined that the adsorbent used is suitable for adsorption. Having an E value of 0.158 kJ/mol in the D-R isotherm indicates that the adsorption is of a physical nature.

Thermodynamic investigations were conducted to determine the spontaneity of the adsorption process. Eq. 8 was utilized to calculate the change in Gibbs free energy of adsorption [18]:

$$\Delta G = \text{-RT } \ln K_L \quad (9)$$

ΔG: Gibbs free energy change (kJ/mol) R: ideal gas constant (8.314 L J mol^{-1} K^{-1})
T: temperature (298 K),

A negative value of ΔG indicates that the process is spontaneous under the given conditions. ΔG value of − 26.58 kJ/mol was obtained for Au(III) adsorption on UV-curable adsorbent. This indicates that the adsorption occurs spontaneously at room temperature.

3.10. Adsorption kinetic

Adsorption kinetics is used to understand the rate and mechanism of the adsorption process and is determined experimentally. This study used pseudo-first-order and pseudo-second-order kinetic Eqs. 8 and 9.

Table 1
Adsorption isotherms data.

Isotherm model and Parameters		
Langmuir	q_{max} (mg/g)	31.15
	K_L (L/mg)	0.232
	R_L	0.801
	R^2	0.9989
Freundlich	1/n	0.0987
	K_f ((mg/g)(L/mg)$^{1/n}$)	18.92
	R^2	0.6972
Temkin	B_T	2.6868
	K_T (L/mg)	665.34
	R^2	0.7114
Dubinin-Radushkevich	q_{max} (mg/g)	30.59
	K_{DR} (mol^2/J^2)	2×10^{-5}
	R^2	0.9541
	E (kJ/mol)	0.158

$$\log(q_e - q_t) = \log\ q_e - \frac{k_1}{2.303}\ t \quad (10)$$

$$\frac{t}{q_t} = \frac{1}{k_2 q_e^2} + \frac{t}{q_e} \quad (11)$$

(q_t is the adsorption capacity at a specific time (mg/g), k_1 and k_2 are the pseudo-first and second order reaction constants respectively (1/min).).

The high correlation coefficient (R^2: 0.982) indicates that the adsorption mechanism (Table 2) of the UV-curable adsorbent fits the pseudo first order model (Fig. S3a-b).

According to the pseudo-second-order kinetic model, the adsorption rate depends on the adsorbent capacity, not the concentration of the adsorbate.

3.11. The effect of foreign ions

The adsorption capacity of the UV-curable adsorbent on Cd(II), Pb (II), and Cu(II) ions was investigated through competitive adsorption tests. The UV-curable adsorbent was submerged in 20 mL of synthetic wastewater at a pH of 1.5 for 6 h, with the ion concentrations in the synthetic wastewater adjusted to 30 mg/L for all ions. The adsorption quantities of Cd(II), Pb(II), Cu(II), and Au(III) ions on the UV-curable adsorbent were determined to be 0.32 mg/g, 0.37 mg/g, 0.31 mg/g, and 17.8 mg/g, respectively. The results from the competitive adsorption tests indicated that the UV-curable adsorbent exhibited a significantly higher adsorption capacity for Au(III) ions compared to Cd(II), Pb (II), and Cu(II).

3.12. Reusability of UV-curable polymeric adsorbent

The UV-curable adsorbent demonstrates reusability, allowing it to be effectively regenerated for up to two cycles. To initiate the regeneration process, the loaded polymeric adsorbent is submerged in a 50 mL solution of 2 M thio-urea at room temperature for 20 min, maintaining a pH of 1.5. Subsequently, the regenerated nanocomposite is dried until it achieves a desorption rate of 89%.

4. Conclusion

This study synthesized a UV-curable polymeric adsorbent by incorporating a Schiff base-containing diacrylate-functionalized oxime-hydrazone monomer, and its adsorption characteristics were reported. The successful synthesis of the monomer was confirmed by ^{1}H NMR and FTIR results. The comparative FTIR characterization of the UV-curable polymeric adsorbent structure showed the absence of specific acrylate and free SH peaks, confirming the cross-linking of all monomers to form a polymeric network. The polymeric adsorbent, except for the diacrylate-functionalized hydrazone-oxime monomer, was prepared by UV-initiated thiol-ene click reaction using trimethylolpropane triacrylate and trimethylolpropane tris(3-mercaptopropionate). TGA investigated the thermal properties of the adsorbent, and it was observed that the cross-linked network started to degrade after reaching 300 °C. This indicates that the structure of the adsorbent remained stable at room temperature, the temperature at which the study was carried out, suggesting that the adsorbent can be used repeatedly at this temperature. The prepared UV-curable adsorbent's surface morphologies and elemental composition were characterized using SEM and SEM-EDAX, respectively. The synthesized polymeric adsorbent

Table 2
Kinetic model parameters.

Pseudo-first-order model			Pseudo-second-order model		
$q_{e(cal)}$ (mg/g)	k_1 (1/min)	R^2	$q_{e(cal)}$ (mg/g)	k_2 (1/min)	R^2
26.56	0.33	0.982	53.76	1.28×10^{-3}	0.5696

exhibited high selectivity and efficiency in adsorbing Au(III) ions from aqueous solutions. The adsorption equilibrium was achieved within 6 h, and the maximum adsorption capacity was determined to be 30.06 mg/g, which is highly competitive among similar adsorbents (Table 1S). The adsorption behavior of Au(III) ions followed pseudo-first-order kinetics, and the Langmuir model described the adsorption isotherm well. Furthermore, the adsorbent demonstrated remarkable selectivity for the adsorption of Au(III) in a simulated wastewater environment over competitive adsorption in an acidic environment. The adsorbent was found to be approximately 60 times more selective when compared to Cd(II), Pb(II), or Cu(II) adsorptions. This developed method offers a fast, easy, and highly selective approach to recovering Au(III) ions from wastewater.

CRediT authorship contribution statement

Oya Aydın Urucu: Investigation, Data curation, Performing adsorption experiments, Writing. **Aslı Beyler Çiğil:** Conceptualization, Polymeric adsorbent synthesis and characterization, Resources, Writing. **Ayşin Zülfikaroğlu:** Conceptualization, Polymeric adsorbent Synthesis and Characterization, Resources, Writing. **kan Esentürk:** Polymeric adsorbent Synthesis and Characterization, Writing – reviewing and editing.

Declaration of Competing Interest

The authors declare that they have no known competing financial interests or personal relationships that could have appeared to influence the work reported in this paper.

Data availability

Data will be made available on request.

Appendix A. Supporting information

Supplementary data associated with this article can be found in the online version at doi:10.1016/j.mtcomm.2023.107270.

References

[1] K.S. Abou Melha, G.A. Al-Hazmi, I. Althagafi, A. Alharbi, A.A. Keshk, F. Shaaban, N. El-Metwaly, Spectral, molecular modeling, and biological activity studies on new schiff's base of acenaphthaquinone transition metal complexes, Bioinorg. Chem. Appl. (2021) 2021.

[2] S. Shahi, H. Roghani-Mamaqani, S. Talebi, H. Mardani, Chemical stimuli-induced reversible bond cleavage in covalently crosslinked hydrogels, Coord. Chem. Rev. 455 (2022), 214368.

[3] X. Yang, Y. Song, Y. Jiang, X. Wang, Y. Yang, J. Wang, Y. Yu, Fabrication and performance of UV–curable Schiff base–containing antibacterial silicone modified materials, Prog. Org. Coat. 174 (2023), 107313.

[4] S.M. Yaseen, B.B. Qasim, N.O. Al-lame, Spectrophotometric determination of Cu (+ II) by complexation with 2-(4-biphenyl) imidazo [1, 2-] pyrimidine-3-hydrazone and studying characteristics of prepared complex, Egypt. J. Chem. 64 (2) (2021) 673–691.

[5] F.A. El-Saied, T.A. Salem, M.M. Shakdofa, A.N. Al-Hakimi, A.S. Radwan, Antitumor activity of synthesized and characterized Cu (II), Ni (II) and Co (II) complexes of hydrazone-oxime ligands derived from 3-(hydroxyimino) butan-2-one, Beni-Suef Univ. J. Basic Appl. Sci. 7 (4) (2018) 420–429.

[6] M. Ahmad, H. Pervez, S. Zaib, M. Yaqub, M.M. Naseer, S.U. Khan, J. Iqbal, Synthesis, biological evaluation and docking studies of some novel isatin-3-hydrazonothiazolines, RSC Adv. 6 (65) (2016) 60826–60844.

[7] W. Kaminsky, J.P. Jasinski, R. Woudenberg, K.I. Goldberg, D.X. West, Structural study of two N (4)-substituted thiosemicarbazones prepared from 1-phenyl-1, 2-propanedione-2-oxime and their binuclear nickel (II) complexes, J. Mol. Struct. 608 (2–3) (2002) 135–141.

[8] S. Mondal, C. Das, B. Ghosh, B. Pakhira, A.J. Blake, M.G. Drew, S. K. Chattopadhyay, Synthesis, spectroscopic studies, X-ray crystal structures, electrochemical properties and DFT calculations of three Ni (II) complexes of aroyl hydrazone ligands bearing anthracene moiety, Polyhedron 80 (2014) 272–281.

[9] Ş. Karadeniz, C.Y. Ataol, O. Şahin, Ö. İdil, H. Bati, Synthesis, structural studies and antimicrobial activity of N′-((2*Z*, 3*E*)-3-(hydroxyimino) butan-2-ylidene)-2-phenylacetohydrazide and its Co (II), Ni (II) complexes, J. Mol. Struct. 1161 (2018) 477–485.

[10] M.M. Al-Ne'aimi, M.M. Al-Khuder, Synthesis, characterization and extraction studies of some metal (II) complexes containing (hydrazoneoxime and bis-acylhydrazone) moieties, Spectrochim. Acta Part A: Mol. Biomol. Spectrosc. 105 (2013) 365–373.

[11] Viswanatha, C., Hymavathi, M., & Devanna, N. (2013, August). ISEANS 194 Direct and Derivative Spectrophotometric Determination of Palladium (II) using 2, 4-dimethoxy Benzaldehyde 4-Hydraoxy Benzoyl Hydrazone (DMBHBH). In *International Congress on Engineering and Information* (p. 258).

[12] V.K. Kumar, M.R. Rao, K.C. Sekhar, N. Devanna, Copper (II) and nickel (II) in Beer, Wine and edible oils, Int. J. Pharma Bio Sci. 1 (2) (2010) 1–8.

[13] S.L. Ferreira, M.A. Bezerra, A.S. Santos, W.N. dos Santos, C.G. Novaes, O.M. de Oliveira, R.L. Garcia, Atomic absorption spectrometry–A multi element technique, TrAC Trends Anal. Chem. 100 (2018) 1–6.

[14] N.A. Kassim, S.A.I.S.M. Ghazali, F.L. Bohari, N.A.Z. Abidin, Assessment of heavy metals in wastewater plant effluent and lake water by using atomic absorption spectrophotometry, Mater. Today.: Proc. 66 (2022) 3961–3964.

[15] F.B. Biswas, I.M. Rahman, K. Nakakubo, M. Endo, K. Nagai, A.S. Mashio, H. Hasegawa, Highly selective and straightforward recovery of gold and platinum from acidic waste effluents using cellulose-based bio-adsorbent, J. Hazard. Mater. 410 (2021), 124569.

[16] O.A. Urucu, A. Aydin, Coprecipitation for the determination of copper (II), zinc (II), and lead (II) in seawater by flame atomic absorption spectrometry, Anal. Lett. 48 (11) (2015) 1767–1776.

[17] L.M. Costa, F.A. Borges, M.H. da Silva Cavalcanti, A.C. do Lago, C.R.T. Tarley, G.D. F.L. Martins, E.C. Figueiredo, Direct magnetic sorbent sampling flame atomic absorption spectrometry (DMSS-FAAS) for highly sensitive determination of trace metals, Anal. Chim. Acta 1251 (2023), 340709.

[18] O.A. Urucu, E.D. Aracier, E. Çakmakçi, Allylimidazole containing OSTE based photocured materials for selective and efficient removal of gold from aqueous media, Microchem. J. 146 (2019) 997–1003.

[19] E. Carasek, A low-cost flame atomic absorption spectrometry method for determination of trace metals in aqueous samples, Talanta 51 (1) (2000) 173–178.

[20] A.U. Oya, Y.G. Zeynep, D. Sabahattin, K.Y. Ece, A. Adnan, A novel ligand for cloud point extraction to determine gold content in ore samples, Environ. Chem. Lett. 12 (3) (2014) 449–453.

[21] Urucu, O.A., Gündüz, Z.Y., & Yetimoğlu, E.K. (2013). Cloud point preconcentration of gold (III) and determination by flame atomic absorption spectrometry.

[22] F.B. Biswas, I.M. Rahman, K. Nakakubo, M. Endo, K. Nagai, A.S. Mashio, H. Hasegawa, Highly selective and straightforward recovery of gold and platinum from acidic waste effluents using cellulose-based bio-adsorbent, J. Hazard. Mater. 410 (2021), 124569.

[23] L. Yuan, N. Zheng, T. Yang, A. Li, Y. Yuan, J. Hua, C. Zhou, Covalent organic polymers with azido group for efficient recovery of gold from gold-bearing waste, J. Taiwan Inst. Chem. Eng. 144 (2023), 104733.

[24] R. Ding, J. Liu, T. Wang, X. Zhang, Bottom-up synthesis of cationic porphyrin-based porous organic polymers for highly efficient and selective recovery of gold, Chem. Eng. J. 449 (2022), 137758.

[25] Y. Chen, Z. Li, R. Ding, T. Liu, H. Zhao, X. Zhang, Construction of porphyrin and viologen-linked cationic porous organic polymer for efficient and selective gold recovery, J. Hazard. Mater. 426 (2022), 128073.

[26] H. Nandivada, X. Jiang, J. Lahann, Click chemistry: versatility and control in the hands of materials scientists, Adv. Mater. 19 (17) (2007) 2197–2208.

[27] J. Collins, Z. Xiao, M. Müllner, L.A. Connal, The emergence of oxime click chemistry and its utility in polymer science, Polym. Chem. 7 (23) (2016) 3812–3826.

[28] Z. Zhang, C. He, X. Chen, Hydrogels based on pH-responsive reversible carbon–nitrogen double-bond linkages for biomedical applications, Mater. Chem. Front. 2 (10) (2018) 1765–1778.

[29] V. Gayathri, K. Stephen, S. Prem, N. Ayyadurai, D. Samanta, Synthesis and catalytic studies of thermoresponsive copper (I) complex towards click reactions, Eur. J. Org. Chem. (2023), e202201182.

[30] E.R. Brisson, Z. Xiao, L. Levin, G.V. Franks, L.A. Connal, Facile synthesis of histidine functional poly (N-isopropylacrylamide): zwitterionic and temperature responsive materials, Polym. Chem. 7 (10) (2016) 1945–1952.

[31] K. Fukuda, M. Shimoda, M. Sukegawa, T. Nobori, J.M. Lehn, Doubly degradable dynamers: dynamic covalent polymers based on reversible imine connections and biodegradable polyester units, Green. Chem. 14 (10) (2012) 2907–2911.

[32] S. Ulrich, D. Boturyn, A. Marra, O. Renaudet, P. Dumy, Oxime ligation: a chemoselective click-type reaction for accessing multifunctional biomolecular constructs, Chem. Eur. J. 20 (1) (2014) 34–41.

[33] J.J. Norman, R.M. Heggie, J.B. Larose, Oximes: I. The synthesis of some substituted 2-oximinoacetophenones, Can. J. Chem. 40 (8) (1962) 1547–1553.

[34] Y. Sang, P.F. Yang, T.D. Li, Selective derivatization of oxime-blocked tolylene-2, 4-diisocyanate, Chin. Chem. Lett. 24 (11) (2013) 1019–1022.

[35] M. Sutradhar, T.R. Barman, J. Klanke, M.G. Drew, E. Rentschler, A novel Cu (II) dimer containing oxime-hydrazone Schiff base ligands with an unusual mode of coordination: Study of magnetic, autoreduction and solution properties, Polyhedron 53 (2013) 48–55.

[36] M.M. Shakdofa, F.A. El-Saied, A.J. Rasras, A.N. Al-Hakimi, Transition metal complexes of a hydrazone–oxime ligand containing the isonicotinoyl moiety: synthesis, characterization and microbicide activities, Appl. Organomet. Chem. 32 (7) (2018) 4376.

[37] S. Hemmati, M. Baghayeri, S. Kazemi, H. Veisi, Biosynthesis of silver nanoparticles using oak leaf extract and their application for electrochemical sensing of hydrogen peroxide, Appl. Organomet. Chem. 32 (11) (2018) 4537.
[38] F. Samy, M. Shebl, Synthesis, spectroscopic, biological, and theoretical studies of new complexes from (*E*)-3-(2-(5, 6- diphenyl-1,2,4- triazin-3- yl)hydrazono)butan-2- one oxime, Appl. Organomet. Chem. 34 (4) (2020) 5502.
[39] A. Zülfikaroğlu, The synthesis, experimental and theoretical characterization of a Pd(II) complex from diacetyl monoxime isobutyrohydrazone, J. Mol. Struct. 1209 (2020), 127950.
[40] A. Stephen, K. Hashmi, C. Lothschutz, F. Rominger, Chlorido[3,30-dibutyl-5,50-(pyridine-2,6-diyl)dipyrazol-1-ido]gold(III), Acta Crystallogr. Sect. E 66 (2010) 64.
[41] V. Levchenko, S. Øien-Ødegaard, D. Wragg, M. Tilset, Crystal structure of (N^C) cyclometalated Au^{III} diazide at 100 K, Acta Crystallogr. Sect. E 76 (2020) 1725–1727.
[42] P.W.R. Corfield, M. Bailey, Crystal structure of dichlorido[2-(diphenylphosphanyl)-3,4,5,6-tetrafluoro-benzene-1-thiolato-2P,S]gold(III), Acta Crystallogr. Sect. E 71 (2015) 181–182.
[43] O. Ozukanar, E. Çakmakçi, G. Sagdic, U.S. Gunay, H. Durmaz, V. Kumbaraci, Eugenol-DOPO: a bio-based phosphorous-containing monomer for thiol-ene photocurable thermosets, J. Polym. Environ. (2023) 1–13.
[44] A. Beyler-Çiğil, H. Cankurtaran, M.V. Kahraman, Photo-crosslinked thiol-ene based hybrid polymeric sensor for humidity detection, React. Funct. Polym. 114 (2017) 75–85.
[45] M. Fırlak, E.K. Yetimoğlu, M.V. Kahraman, Adsorption of Au (III) ions from aqueous solutions by thiol-ene photoclick hydrogels and its application to electronic waste and geothermal water, J. Water Process Eng. 3 (2014) 105–116.
[46] A. Beyler Çiğil, O. Aydın Urucu, H. Birtane, M.V. Kahraman, Cellulose/cysteine based thiol-ene UV cured adsorbent: removal of silver (I) ions from aqueous solution, Cellulose 28 (10) (2021) 6439–6448.
[47] S. Gopi, A. Pius, R. Kargl, K.S. Kleinschek, S. Thomas, Fabrication of cellulose acetate/chitosan blend films as efficient adsorbent for anionic water pollutants, Polym. Bull. 76 (2019) 1557–1571.
[48] N.P. Finkelstein, R.D. Hancock, A new approach to the chemistry of gold, Gold. Bull. 7 (3) (1974) 72–77.
[49] H. Birtane, O.A. Urucu, N. Yıldız, A.B. Çiğil, M.V. Kahraman, Statistical optimization and selective uptake of Au (III) from aqueous solution using carbon nanotube-cellulose based adsorbent, Mater. Today Commun. 30 (2022), 103144.
[50] Z.Ç. Okumuş, T.H. Doğan, Removal of water from biodiesel with resin: isothermal, kinetic and thermodynamic investigation of adsorption, Eur. J. Sci. Technol. 15 (2019) 561–570.